Field-induced XY behavior in the $S=\frac{1}{2}$ antiferromagnet on the square lattice

Alessandro Cuccoli,[1,2] Tommaso Roscilde,[1,2] Ruggero Vaia,[3,2] and Paola Verrucchi[1,2]

[1]*Dipartimento di Fisica dell'Università di Firenze—via G. Sansone 1, I-50019 Sesto Fiorentino (FI), Italy*
[2]*Istituto Nazionale per la Fisica della Materia—U.d.R. Firenze—via G. Sansone 1, I-50019 Sesto Fiorentino (FI), Italy*
[3]*Istituto di Fisica Applicata "Nello Carrara" del Consiglio Nazionale delle Ricerche—via Panciatichi 56/30, I-50127 Firenze, Italy*

Making use of the quantum Monte Carlo method based on the worm algorithm, we study the thermodynamic behavior of the $S=\frac{1}{2}$ isotropic Heisenberg antiferromagnet on the square lattice in a uniform magnetic field varying from very small values up to the saturation value. The field is found to induce a Berezinskii-Kosterlitz-Thouless transition at a finite temperature, above which genuine XY behavior in an extended temperature range is observed. The phase diagram of the system is drawn, and the thermodynamic behavior of the specific heat and of the uniform and staggered magnetization is discussed in sight of an experimental investigation of the field-induced XY behavior.

Field-induced effects in low-dimensional antiferromagnets have been the subject of renewed interest in the last few years; while on the experimental side fields of very high intensity have become available, on the theoretical side the possibility of inducing novel magnetic phases via application of a strong field has been pointed out.[1,2]

In this paper we consider the two-dimensional quantum Heisenberg antiferromagnet (2D QHAF) in a uniform magnetic field, described by the Hamiltonian

$$\hat{\mathcal{H}} = \frac{J}{2} \sum_{i,d} \hat{\boldsymbol{S}}_i \cdot \hat{\boldsymbol{S}}_{i+d} - g\mu_B H \sum_i \hat{S}_i^z, \qquad (1)$$

where $\boldsymbol{i}=(i_1,i_2)$ runs over the sites of a square lattice, $\boldsymbol{d}$ connects each site to its four nearest neighbors, $J>0$ is the antiferromagnetic exchange coupling, H is the applied Zeeman field, and $|S|^2=S(S+1)$. We will hereafter use reduced temperature and magnetic field, $t \equiv T/J$ and $h \equiv g\mu_B H/(JS)$. Nonmagnetic systems as the Bose-Hubbard model[3] and the related superfluid problem[4] can also be mapped onto Hamiltonian (1).

The rich phenomenology[5] of the model is ruled by the interplay between the exchange and the Zeeman terms in Eq. (1). The applied field breaks the $O(3)$ symmetry of the isotropic model and induces a uniform alignment in the z direction; such alignment frustrates the antiferromagnetic order along z but does not clash with antialignment on the xy plane, where $O(2)$ symmetry stays untouched. For infinitesimally small fields one hence expects the spins to lay antialigned on the xy plane, and progressively cant out of it as h is increased. Saturation occurs at the critical value $h_c=8$, above which the ground state displays uniform ferromagnetic alignment along the z direction. In the range $0<h<h_c$ one may also expect thermal fluctuations of the z spin components to be smaller for a larger field, while no such reduction should occur as far as the x and y components are concerned. The above picture clearly suggests the model to share essential features with the easy-plane 2D QHAF.[6]

In the classical limit ($S\to\infty$, $JS^2\to J_{cl}$, $g\mu_B H\to h\,J_{cl}$) both analytical[7,8] and numerical[9] calculations revealed the occurrence of a Berezinskii-Kosterlitz-Thouless (BKT)

transition,[10,11] for all values of h below saturation. In the quantum $S=\frac{1}{2}$ case, evidence of a field-induced BKT transition was recently achieved for small fields by means of quantum Monte Carlo (QMC) simulations based on the continuous-time loop algorithm.[2] Unfortunately, the loop algorithm loses its efficiency exponentially as the field and/or the inverse temperature are increased:[12] this fact has so far prevented a systematic investigation of the strong-field regime.[13] However, the recently proposed *worm*[6] (or *directed-loop*[14]) algorithm, working in any lattice dimension, is effective also in the presence of a uniform field of arbitrary intensity. Our QMC simulations are in fact based on such an algorithm, which is a pure-quantum cluster algorithm (by this we mean that it has no classical analog, so far), which takes the field into account by the dynamical nature of the process of cluster (worm) growth, with the possibility that the worm traces back its route after *bouncing* at some point. In particular, the update process is irreversible (i.e., the inverse of a single update step with finite probability can have a vanishing probability), thus reflecting the time-reversal symmetry breaking due to the presence of the field. A detailed description of the algorithm is beyond the scope of this paper and can be found in Ref. 15. Our simulations were performed on a $L\times L$ square lattice ($L=16$, 32, 64, and 96), each consisting of 10^4 MC steps for thermalization and of $(1-1.5)\times10^5$ MC steps for evaluation of thermodynamic observables. During thermalization, the number of worms produced at each step is adjusted so that the total length of the worms in the imaginary-time direction roughly equals the size of the $(2+1)$-dimensional lattice, L^2/t; this number is then kept fixed during the measurement phase. In this way, autocorrelation times of the order of unity are achieved for all values of the field.

Thanks to this very effective tool, we got access to the thermodynamic behavior of model (1) with $S=\frac{1}{2}$ and h varying from 0 to h_c, looking for signatures of field-induced BKT behavior that can be the object of experimental observation. In particular, we have focused our attention on the specific heat $c(t,h)$ and the field-induced uniform magnetization $m_u^z(t,h)$, which are easily accessible to experiments, as well as on the staggered magnetization along the field axis

TABLE I. $t_{BKT}(h)$ as obtained by finite-size scaling analysis.

h	t_{BKT}
0.1	0.175(5)
0.2	0.195(5)
0.4	0.213(5)
1.0	0.254(5)
2.0	0.292(5)
4.0	0.282(5)
6.0	0.202(5)

$m_{s,L}^z(t,h)$, which provides further insight into the microscopic ordering mechanism. Seven values of the field have been considered: $h = 0.1$, 0.2, 0.4, 1, 2, 4, and 6.

First of all we have performed a detailed finite-size scaling analysis in order to check whether or not the predicted critical scaling behavior of the in-plane staggered susceptibility[11] and of the helicity modulus[16] are reproduced at consistent temperatures: having got a positive answer, we may state that a finite-temperature phase transition of BKT type occurs in the model for all the considered field values. The estimate of the critical temperature corresponding to each field has been obtained via the same procedure used in Ref. 6 for the easy-plane 2D QHAF: the resulting values are listed in Table I; they are consistent with previous results[2] for $h = 0.2$ and $h = 0.4$. In Fig. 1 we report the phase diagram of the model for $S = \frac{1}{2}$ and $S = \infty$, the latter as from classical MC results.[9] We observe that the effect of quantum fluctuations is limited to a strong renormalization of t_{BKT} with respect to the classical case, but the field dependence is qualitatively the same.

Let us first concentrate on the weak-field regime: from various analytical arguments[8,17,18] one can infer a mapping of
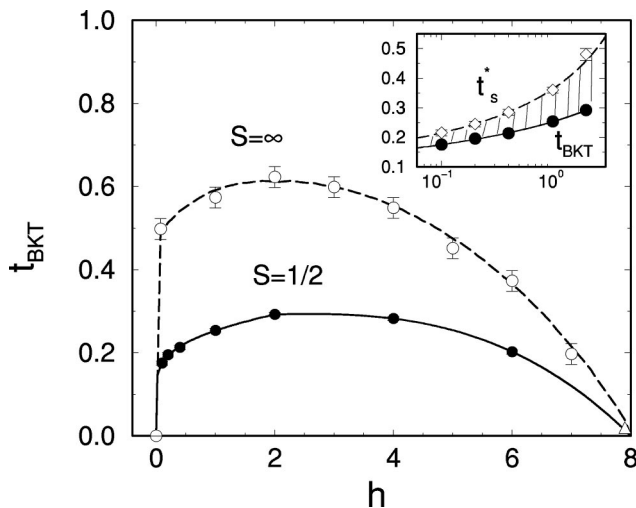
FIG. 1. Phase diagram of the $S = \frac{1}{2}$ 2D QHAF in a magnetic field. Open symbols refer to the classical limit of the model, from Ref. 9; the triangle is a QMC result from Ref. 13. Inset: $t_{BKT}(h)$ and $t_s^*(h)$ (see text) for weak fields; solid and dashed lines are logarithmic fits to the first three points of each dataset, and the shaded area marks the region of disordered XY behavior.

the 2D QHAF in a field on a weakly easy-plane magnet with exchange anisotropy, i.e., Hamiltonian (1) with $H = 0$ and the additional term $-J\Delta\Sigma_{i,d}\hat{S}_i^z\hat{S}_{i+d}^z$; the effective exchange anisotropy Δ is expected to scale with the field as $\Delta \propto h^2$. Hence, the BKT critical temperature is expected to obey, both in the classical and in the quantum case,[6] the following expression

$$t_{BKT}(h) \simeq \frac{4\pi\rho_S/J}{\ln(C/h^2)}, \quad (2)$$

where ρ_S is the spin stiffness of the isotropic model, and C a constant. Fitting our results for the lowest three values of h to the above expression we get $\rho_S \simeq 0.22J$, and excluding the third value we find $\rho_S \simeq 0.19$. Remarkably, these values are consistent with the renormalized spin stiffness of the $S = \frac{1}{2}$ isotropic 2D QHAF, $\rho_S = 0.180J$.[19] We also notice that the fitting curve keeps interpolating the data up to $h \lesssim 2$. Finally, by directly comparing the low-field behavior of $t_{BKT}(h)$ with that of $t_{BKT}(\Delta)$ in the weakly planar antiferromagnet,[6] we obtain an excellent agreement for $\Delta \approx 0.1h^2$.

Moving towards higher fields two different effects are expected: (i) the fluctuations of the z components become smaller, resulting in an enhanced effective easy-plane anisotropy, and (ii) the average projection of the spins in the xy plane decreases, due to the increasing uniform magnetization. Globally, the system behaves as a *renormalized* planar rotator with progressively *reduced* rotator length. It is remarkable that, despite the spin configurations being characterized by a smaller and smaller projection in the xy plane, the XY character is apparent even for h close to h_c and the transition verifies all the predictions of the BKT theory. The interplay between the two competing field effects yields the nonmonotonous dependence of $t_{BKT}(h)$: for low field the reduction of z fluctuations is dominant and $t_{BKT}(h)$ increases with h, starting as in Eq. (2), while for higher field spin canting prevails and $t_{BKT}(h)$ decreases, eventually vanishing at the saturation field h_c. Therefore, a maximum in $t_{BKT}(h)$ connects the two limiting behaviors, as already observed in the classical phase diagram: the comparison in Fig. 1 shows that for $S = \frac{1}{2}$ the maximum shifts to slightly higher field as a consequence of quantum fluctuations.

We now consider the temperature dependence of some relevant observables, beginning with the specific heat $c(t,h)$. While our data resolution for $h \lesssim 0.4$ prevents from observing significant deviations with respect to the zero-field system, the results for the four largest fields are shown in Fig. 2; in particular, what is plotted is the specific heat variation upon application of the field, $\Delta c(t,h) = [c(t,h) - c(t,0)]$, divided by t. This quantity equals the difference of the entropy derivatives $\partial_t S(t,h) - \partial_t S(t,0)$ and allows us to draw the following picture. At low temperature the entropy increase is smaller than in zero field, reflecting the presence of quasi-long-range order induced by the field via stabilization of bound vortex/antivortex pairs. Slightly above the BKT transition (t about 20–30 % larger) a sharp entropy increase occurs, which we interpret as due to vortex unbinding. When the temperature is further raised all vortices are
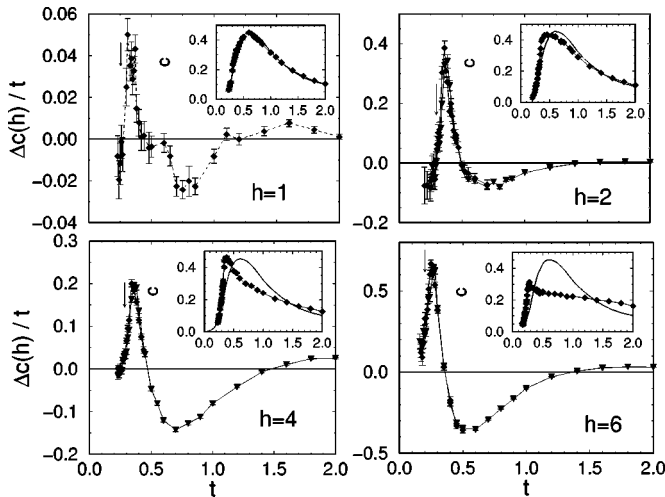
FIG. 2. $\Delta c(t,h)/t = [c(t,h) - c(t,0)]/t$ vs temperature, for four different field values. Insets: magnetic specific heat $c(t,h)$ compared to $c(t,0)$ (thick solid line). The zero-field specific heat $c(t,0)$ is obtained by interpolating numerical and analytical data from Refs. 20–22; the arrows mark the estimated BKT critical temperatures.

free and then $S(t,h)$ increases slower than $S(t,0)$; eventually the entropy difference vanishes in the fully disordered system at $t \rightarrow \infty$. For increasing field the peak of $c(t,h)$, which mimics the BKT peak of the *XY* model, moves to lower temperature, thereby getting narrower, as shown in the insets of Fig. 2. It is worth noting that $\Delta c(t,h)$, which bears very clear signatures of the BKT behavior, is easily accessible to experiments, because nonmagnetic contributions cancel in its definition.

We have also considered the field-induced uniform magnetization, $m_u^z(t,h) \equiv \langle \hat{S}_i^z \rangle$; such a quantity, which can be experimentally determined via standard magnetometry measurements, is also a highly precise output of the QMC simulations. In Fig. 3 we report $m_u^z(t,h)/h$ for different fields. For $h \lesssim 2$ and for high enough temperature this quantity is found to coincide with the uniform susceptibility of
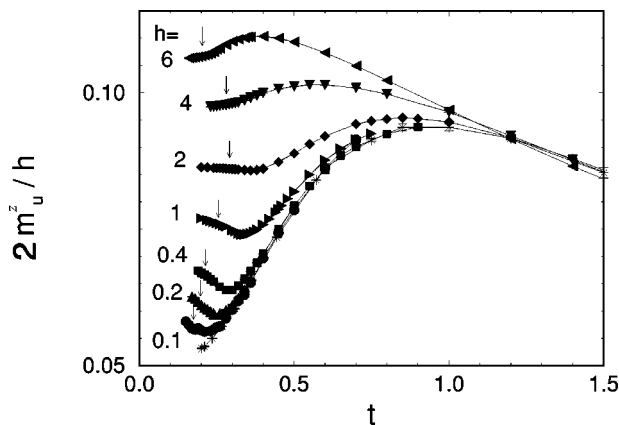
FIG. 3. Field-induced uniform magnetization $m_u^z(t,h)$ vs temperature, for different field values. The stars represent the zero-field uniform susceptibility from Refs. 22 and 20; arrows as in Fig. 2.
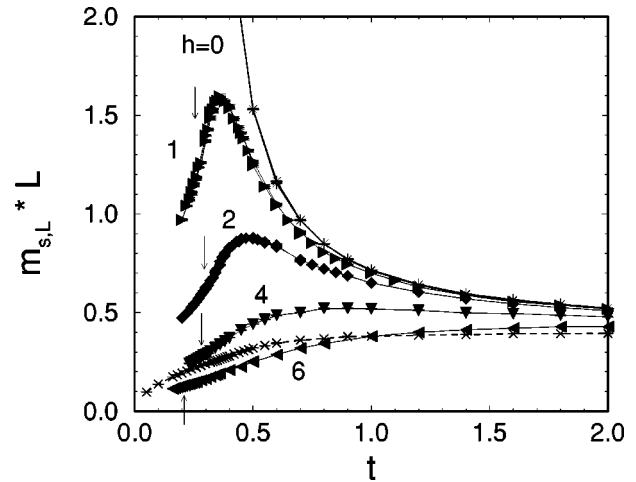
FIG. 4. Finite-size staggered magnetization $m_{s,L}^z(t,h)$ vs temperature, for different field values. The ×'s represent the same quantity for the $S=\frac{1}{2}$ 2D *XY* model. Arrows as in Fig. 2.

the zero-field case, thus showing that the magnetization process is linear. Upon lowering t the nonlinearities show up and the uniform magnetization changes completely its temperature dependence, displaying a minimum at $t = t_u^*(h)$. This feature marks the onset of *XY* behavior: as the temperature is lowered below t_u^*, the system is increasingly magnetized along the z axis and the short-range antiferromagnetic correlations of the z spin components, as well as their thermal fluctuations, are suppressed, in turn stabilizing the canted configurations. A remarkable feature is that this crossover to *XY* behavior is located at a temperature $t_u^*(h)$ well above the critical point. For $h \gtrsim 2$ the minimum above t_{BKT} disappears, and the most prominent feature is rather the shift of the broad maximum to lower temperature.

The crossover from isotropic to *XY* behavior in low fields ($h \lesssim 2$) can be also detected in the temperature dependence of the finite-size staggered magnetization along the hard z axis,[23] $m_{s,L}^z(t,h) \equiv L^{-2} \langle |\Sigma_i (-)^i \hat{S}_i^z| \rangle$, shown in Fig. 4. In absence of long-range order $m_{s,L}^z$ is known to scale to zero as $1/L$ (for large enough L),[24] and $m_{s,L}^z L$ is hence a bulk property of the system. In the limit $t \rightarrow \infty$ the system behaves as a collection of paramagnetic spins so that, by applying the central-limit theorem, one finds $m_{s,L}^z L \rightarrow \sqrt{2S(S+1)/(3\pi)} \approx 0.399$ for $S=\frac{1}{2}$. As t decreases, $m_{s,L}^z L$ in the isotropic 2D QHAF monotonically increases and diverges for $t \rightarrow 0$. In the 2D *XY* model the same quantity decreases below the infinite-t value, due to the suppression of out-of-plane fluctuations. The coexistence of both the above behaviors is most clearly observed for $h \lesssim 2$, and the appearance of a maximum in $m_{s,L}^z$ at $t \equiv t_s^*$ also marks the crossover from isotropic to *XY* behavior.

Hitherto, we have identified two ways of locating a crossover temperature, at least for low and intermediate fields. One can check that for low fields these temperatures match with each other, $t_s^*(h) \simeq t_u^*(h)$, so that the crossover temperature is unambiguous and its estimates are $t_s^*(0.1) = 0.22(1)$, $t_s^*(0.2) = 0.25(1)$, and $t_s^*(0.4) = 0.29(1)$. In this regime the crossover temperature is expected to follow a

logarithmic behavior analogous to that of Eq. (2) (with a different coefficient C') as suggested in Refs. 6 and 23; a fit of $t_s^*(h)$ for $h \lesssim 0.4$ gives $\rho_S = 0.19$, again in good agreement with the known value[19] of the spin stiffness for $S = \frac{1}{2}$. For larger fields $t_s^*(h)$ is systematically higher than $t_u^*(h)$, suggesting that the crossover phenomenon extends over a wider temperature range, but we note that for intermediate fields the same fitting function still interpolates the data, $t_s^*(1) = 0.36(1)$ and $t_s^*(2) = 0.48(2)$, as shown in the inset of Fig. 1. Finally, for strong fields the explicit signature of the crossover gradually disappears from $m_{s,L}^z * L$, and for $h = 6$ this quantity is nearly monotonic as in the XY model; the antiferromagnetic interaction of the z components is almost completely overcome by the applied field.

In conclusion, we have studied the $S = \frac{1}{2}$ two-dimensional QHAF on the square lattice in an arbitrary uniform field by means of the quantum Monte Carlo method based on the worm algorithm. Our results point out that an arbitrarily small field is able to induce a BKT transition and an extended XY phase above it, as in the case of an easy-plane

exchange anisotropy. The field-induced XY behavior becomes more and more marked for increasing fields, while for strong fields the antiferromagnetic behavior along the field axis is nearly washed out, so that the system behaves as a planar rotator model with antiferromagnetism surviving in the orthogonal plane only; the BKT critical temperature vanishes as the field reaches the saturation value h_c and the effective rotator length goes to zero. The model in a moderately strong field represents an ideal realization of the XY model: XY behavior can be detected by measuring standard non-critical quantities, as the specific heat or the induced magnetization; this opens the possibility for an experimental realization of the XY model in purely magnetic systems, and for a systematic investigation of the dynamics of vortex/antivortex excitations.

[1] See *High Magnetic Fields: Applications in Condensed Matter Physics and Spectroscopy*, Lecture Notes in Physics Vol. 595, edited by C. Berthier, L.-P. Levy, and G. Martinez (Springer-Verlag, Heidelberg, 2002); S. Yunoki, Phys. Rev. B **65**, 092402 (2002); G. Schmid, S. Todo, M. Troyer, and A. Dorneich, Phys. Rev. Lett. **88**, 167208 (2002).

[2] M. Troyer and S. Sachdev, Phys. Rev. Lett. **81**, 5418 (1998).

[3] R.T. Scalettar, G.G. Batrouni, A.P. Kampf, and G.T. Zimanyi, Phys. Rev. B **51**, 8467 (1995).

[4] M.P.A. Fisher, P.B. Weichman, G. Grinstein, and D.S. Fisher, Phys. Rev. B **40**, 546 (1989).

[5] *Magnetic Properties of Layered Transition Metal Compounds*, edited by L.J. de Jongh (Kluwer, Dordrecht, 1990); H.J.M. de Groot and L.J. de Jongh, Physica B **141**, 1 (1986); L.J. de Jongh, H.B. Brom, H.J.M. de Groot, Th.W. Hijmans, and W.H. Korving, J. Magn. Magn. Mater. **54–57**, 1447 (1986).

[6] A. Cuccoli, T. Roscilde, V. Tognetti, R. Vaia, and P. Verrucchi, Phys. Rev. B **67**, 104414 (2003).

[7] J. Villain and J.M. Loveluck, J. Phys. (France) Lett. **38**, L77 (1977).

[8] A.S.T. Pires, Phys. Rev. B **50**, 9592 (1994).

[9] D.P. Landau and K. Binder, Phys. Rev. B **24**, 1391 (1981).

[10] V.L. Berezinskii, Zh. Éksp. Teor. Fiz. **59**, 907 (1970) [JETP **32**, 493 (1971)].

[11] J.M. Kosterlitz and D.J. Thouless, J. Phys. C **6**, 1181 (1973); J.M. Kosterlitz, *ibid.* **7**, 1046 (1974).

[12] H. Onishi, M. Nishino, N. Kawashima, and S. Miyashita, J. Phys. Soc. Jpn. **68**, 2547 (1999).

[13] A modified loop algorithm suitable for a strong field is applied for $h = 7.9$ and lattices up to 20×20 in: O.F. Syljuåsen, Phys. Rev. B **61**, 846 (2000).

[14] O.F. Syljuåsen and A.W. Sandvik, Phys. Rev. E **66**, 046701 (2002).

[15] T. Roscilde, Ph.D. dissertation, Università di Pavia, 2002.

[16] P. Olsson and P. Minnhagen, Phys. Scr. **43**, 203 (1991).

[17] Y. Okwamoto, J. Phys. Soc. Jpn. **53**, 2434 (1984).

[18] M.E. Zhitomirsky and T. Nikuni, Phys. Rev. B **57**, 5013 (1998).

[19] B.B. Beard, R.J. Birgeneau, M. Greven, and U.-J. Wiese, Phys. Rev. Lett. **80**, 1742 (1998).

[20] J.-K. Kim and M. Troyer, Phys. Rev. Lett. **80**, 2705 (1998).

[21] M. Takahashi, Phys. Rev. B **40**, 2494 (1989).

[22] M.S. Makivić and H.-Q. Ding, Phys. Rev. B **43**, 3562 (1991).

[23] A. Cuccoli, T. Roscilde, R. Vaia, and P. Verrucchi, Phys. Rev. Lett. **90**, 167205 (2003).

[24] K. Binder and D. W. Heermann, *Monte Carlo Simulation in Statistical Physics—An Introduction* (Springer, Berlin, 1988).